Simultaneous Height and Adhesion Imaging of Antibody-Antigen Interactions by Atomic Force Microscopy

Oscar H. Willemsen,* Margot M. E. Snel,*§ Kees O. van der Werf,* Bart G. de Grooth,* Jan Greve,* Peter Hinterdorfer,# Hermann J. Gruber,# Hansgeorg Schindler,# Yvette van Kooyk,§ and Carl G. Figdor*§
*Department of Applied Physics, Applied Optics Group, University of Twente, Enschede, The Netherlands; #Institute for Biophysics, University of Linz, Linz, Austria; and §Department of Tumor Immunology, University Hospital Nijmegen, Nijmegen, The Netherlands

ABSTRACT Specific molecular recognition events, detected by atomic force microscopy (AFM), so far lack the detailed topographical information that is usually observed in AFM. We have modified our AFM such that, in combination with a recently developed method to measure antibody-antigen recognition on the single molecular level (Hinterdorfer, P., W. Baumgartner, H. J. Gruber, K. Schilcher, and H. Schindler, *Proc. Natl. Acad. Sci. USA* 93:3477–3481 (1996)), it allows imaging of a submonolayer of intercellular adhesion molecule-1 (ICAM-1) in adhesion mode. We demonstrate that for the first time the resolution of the topographical image in adhesion mode is only limited by tip convolution and thus comparable to tapping mode images. This is demonstrated by imaging of individual ICAM-1 antigens in both the tapping mode and the adhesion mode. The contrast in the adhesion image that was measured simultaneously with the topography is caused by recognition between individual antibody-antigen pairs. By comparing the high-resolution height image with the adhesion image, it is possible to show that specific molecular recognition is highly correlated with topography. The stability of the improved microscope enabled imaging with forces as low as 100 pN and ultrafast scan speed of 22 force curves per second. The analysis of force curves showed that reproducible unbinding events on subsequent scan lines could be measured.

INTRODUCTION

The invention of the scanning probe microscopes (Binnig et al., 1983; 1986) has stimulated the study of objects on a nanometer scale. The atomic force microscope (AFM) has become the most popular and suitable one in life science since Marti and co-workers (1987) demonstrated the operation in liquid. This paved the way for measurements on a variety of biological samples, ranging from living cells (Henderson et al., 1992; Putman et al., 1994) to the activity of single molecules (Radmacher et al., 1994a; Kasas et al., 1997). The potential of AFM to measure intermolecular forces down to the pN range was first shown by Hoh and co-workers (1992). In addition, this force sensitivity was used to quantify the unbinding forces of individual ligand-receptor pairs (Florin et al., 1994; Lee et al., 1994a, b; Moy et al., 1994; Dammer et al., 1995) applying the so-called force-distance mode. This method was extended by Rief and co-workers (1997a, b) who could demonstrate the repetitive conformational changes of individual molecules by stretching individual titin molecules while maintaining the binding between tip and molecule. Also, measurement of antibody-antigen interactions came within range with either the antigen (Dammer et al., 1996; Allen et al., 1997) or the antibody on the tip (Hinterdorfer et al., 1996; Hinterdorfer et al., 1998). The latter approach significantly benefited from the application of spacer technology that enhanced motility and flexibility of the antibodies and enabled discrimination between specific and nonspecific unbinding events (Hinterdorfer et al., 1996).

The simultaneous image formation and force measurement (Radmacher et al., 1994b; van der Werf et al., 1994; Berger et al., 1995) is called adhesion mode AFM and it is a new promising tool to map binding sites of molecules. A first attempt in single molecular force mapping was carried out by Hinterdorfer and co-workers (1996), who mapped the interaction probability of an antibody-antigen pair as a function of lateral distance and determined the position of the antigens with 1.5-nm accuracy. Another promising approach (Ludwig et al., 1997) simultaneously maps the height and adhesion of a photographically patterned surface of streptavidin and gold.

In this paper we have studied the adhesion molecule ICAM-1, a ligand of the adhesion receptor leukocyte function-associated antigen-1 (LFA-1). Both molecules play an important role in mediating cell adhesion of cells of the immune system (Figdor et al., 1990). We and others have found that these adhesion interactions are tightly controlled by the cell, among others by conformational changes resulting in affinity alterations (Diamond and Springer, 1994; Hynes, 1992; Lub et al., 1995). To get a better understanding of the dynamics of LFA-1-ICAM-1 interactions we have chosen to use AFM to investigate isolated ICAM-1 and LFA-1 molecules. Here we studied the distribution of isolated ICAM-1 molecules on a mica surface and the capacity of anti-ICAM-1 antibodies on tips to detect individual ICAM-1 molecules on surfaces. The AFM was modified such that it, for the first time, allowed on-line mapping of the height of single ICAM-1 molecules simultaneously with the adhesion image. The contrast in the adhesion image is

Received for publication 12 November 1997 and in final form 7 July 1998.
Address reprint requests to Dr. Carl G. Figdor, Department of Tumor Immunology, University Hospital Nijmegen, 6525 EX Nijmegen, The Netherlands. Tel.: 31-24-3617600; Fax: 31-24-3540339; E-mail: c.figdor@dent.kun.nl.

0006-3495/98/11/2220/09 $2.00

attributed to the single molecular recognition between ICAM-1 and the anti-ICAM-1 antibody and was significantly enhanced by the use of spacer technology, developed earlier (Hinterdorfer et al., 1996). In addition, recording of the force curve facilitated the discrimination between specific and nonspecific recognition events.

MATERIALS AND METHODS

Substrate and tip preparation

In this study a soluble fragment of ICAM-1 is used to prepare substrates. This sICAM-1 possesses essentially the entire five extracellular domains of the transmembrane ICAM-1 molecule. Human sICAM-1 was purified from tissue culture supernatant of transfected Chinese hamster ovary-K1 cells by immunoaffinity chromatography, as described (Binnerts, manuscript in preparation). The purity of the sICAM-1 preparation was confirmed using SDS-polyacrylamide gel electrophoresis (data not shown). The concentration of the sICAM-1 preparation was determined in a sandwich ELISA using the anti-ICAM-1 antibody, F10.2.

Substrates were prepared by adsorption of sICAM-1 from either a 0.3 mg/ml solution (for high surface concentration) or a 0.06 mg/ml solution (for low surface concentration) to freshly cleaved mica. After incubation for 10 min at room temperature, the mica substrate was rinsed extensively with phosphate buffered saline (PBS; Gibco, Life Technologies B.V., Breda, The Netherlands) to remove any loosely bound protein. The PBS consisted of 137 mM NaCl, 2.7 mM KCl, 8.1 mM Na_2HPO_4, 1.5 mM KH_2PO_4, and 0.5 mM $MgCl_2$, pH 7.3.

For the preparation of the sample suitable for adhesion mode imaging at low surface concentration, freshly cleaved mica was functionalized with amine-containing groups as described (Hinterdorfer et al., 1996). All subsequent steps were performed in the dark. The amine-functionalized mica was incubated for 16 h in a solution of 0.75 mM *N*-5-azido-2-nitrobenzoyloxysuccimide (ANB-NOS, a photoreactive linker) and 120 mM triethylamine in dimethylformamide (DMF). After the incubation the mica was washed with DMF, DMF:$CHCl_3$ (1:1), and $CHCl_3$ to remove the excess ANB-NOS. sICAM-1 was coupled to the modified mica by adsorption for 10 min from a 0.3 mg/ml solution at room temperature followed by irradiation of the substrate with a 100 W mercury high-pressure lamp equipped with a UG11 filter for 10 min. The intensity at the irradiated spot was determined to be 1×10^3 W/m^2. To prevent protein damage by short wavelength UV radiation the substrate was covered with glass. Loosely bound protein was removed by shaking the substrate for 16 h in 1% SDS/PBS and by extensive rinsing with PBS. Substrates were kept under buffer.

The purified anti-ICAM-1 mouse monoclonal antibody, F10.2 (Bloemen et al., 1992) was covalently attached to silicon nitride tips (Park Scientific Instruments, Sunnyvale, CA) via a spacer, i.e., an 8-nm-long polyethylene glycol derivative with an amine-reactive end and a thiol-reactive end, essentially as described previously (Haselgrübler et al., 1995; Hinterdorfer et al., 1996). This protocol allows detection of single antibody-antigen recognition events, because the antibody concentration on the tips is chosen such that on average only one antibody on the tip has access to the antigen on the surface. The functionalized tips were stored in PBS containing 0.01% sodium azide at 4°C. The density of antibodies coupled to the tips was determined from topographical images (tapping mode) of flat Si_3N_4 substrates functionalized simultaneously (in the same preparation) with the tips, yielding 250–375 antibodies per μm^2. These values correspond to 0.5–0.75 antibodies per area of the tip end (2000 nm^2, as estimated from the nominal tip radius of 20 nm and from the length of the spacer-antibody complex of 15 nm). This value agrees very well with the antibody density, previously obtained via high-resolution fluorescence microscopy (Hinterdorfer et al., 1996; Schmidt et al., 1996).

To show the specificity of the antibody-antigen interactions, measurements were carried out with tips to which an irrelevant antibody, TS2/4, was attached by the spacer. The mouse monoclonal antibody TS2/4, which recognizes LFA-1 (Sanchez-Madrid et al., 1982), was purified from the tissue culture supernatant by protein A affinity chromatography. The antibody-antigen interactions were specifically blocked with a solution of F10.2-antibody at a final concentration of 17.5 μg/ml. In one case, before the specific blocking a "nonspecific blocking" step was applied with a solution of the irrelevant TS2/4-antibody at a final concentration of 17.5 μg/ml. After the addition of the antibodies F10.2 or TS2/4 the solution was incubated for at least 10 min before AFM measurements were carried out.

Use of adhesion imaging techniques for specific interactions

Our stand-alone AFM (van der Werf et al., 1993) was optimized for the measurements of single molecular interactions. The lateral displacement spindles were removed and the size of the piezo tube (Stavely Sensors, East Hartford, CT) was decreased for better mechanical and thermal stability. For the measurements on fragile biomolecules in liquid two modes of operation were used.

Tapping mode (Zhong et al., 1993; Hansma et al., 1994; Putman et al., 1994) was used for high-resolution imaging the topography of proteins in buffer. V-shaped cantilevers (MICROLEVERS, tip F, Park Scientific Instruments, Sunnyvale, CA) with a spring constant of 500 pN/nm were operated at frequencies between 18 and 24 kHz. For the low concentration image an e-beam deposited (EBD) tip was grown on top of the original tip for higher aspect ratio and less adhesion (Keller and Chic-Chung, 1992; de Grooth and Putman, 1992). Damping was minimized to 5% to avoid damage of the sample. Images contain 300×300 pixels and were recorded at a line frequency of 4 Hz.

For simultaneous measurements of topography and adhesion the force-distance mode was used. To get a low and stable applied force, a modified version of the original force-distance module (van der Werf et al., 1994) was used. In the design of the hardware electronics a piezo actuator was ramped up and down. When the surface was reached the cantilever deflected until a preset deflection set-point was reached. The set-point was set relative to the electronic ground level in the original design, and thermal drifts in the deflection signal resulted in variations of both the applied force and measured adhesion. In our improved design the thermal drift of the deflection signal was removed by storing a low-pass filtered (9 Hz) deflection signal in a sample/hold circuit at the beginning of a force-distance curve measurement. This value was then subtracted from the raw deflection signal to give a drift-compensated signal. The resulting signal was fed into two circuits. The first one has a peak detector for adhesion recording, while the second one is a low-pass filter with a bandwidth of 250 Hz, which is still fast enough to follow the relatively slow force-distance measurements. In this way imaging with stable maximal applied forces as small as 100 pN was accomplished. A high-pass filter of 1 Hz was used to eliminate the 1/f noise in the height measurement. For single molecular height resolution further reduction of the 1/f noise was needed. The main contribution of the 1/f noise was the thermal expansion of the complete AFM head, caused by the airflow near the head. By covering the AFM head with an airtight container and waiting for 15 min to reach thermal equilibrium, high-pass filtering with only 0.1 Hz resulted in a height stability of 0.2 nm rms. For on-line analysis both height and adhesion images were recorded. In addition, the dynamic process of adhesion was analyzed by recording the whole force-distance curve for every pixel of the scan. This was done by sampling the deflection signal with 1000 points per force-distance curve, leading to a sampling rate of 13 kHz. These data were used for off-line analysis of individual force-distance curves on specific sites.

All adhesion measurements were done with a rectangular cantilever (MICROLEVERS, tip B, Park Scientific Instruments, Sunnyvale, CA). The force constant was determined with the thermal noise method (Florin et al., 1995; Butt and Jaschke, 1995). Values ranged from 13 to 46 pN/nm. The piezo tube was ramped up and down with an amplitude of 180 nm and a frequency of 13 Hz. The height stabilization by reducing the airflow allowed a further reduction of the amplitude to 120 nm and an increase of the pixel frequency to 22 Hz, a factor of eight higher than in any previous

antibody-antigen experiment. The frequency was limited by the viscous drag of the cantilever in buffer. For a 100 × 100 pixel scan this resulted in a measurement time of 14 min per image for Fig. 2, *a–h*, and 8 min for Fig. 2, *i* and *j*.

RESULTS

Imaging of single ICAM-1 molecules

Fig. 1 shows ICAM-1 molecules on a mica substrate imaged in tapping mode at low (*a*) and high (*b*) concentration. The low concentration image shows randomly distributed ICAM-1 molecules with a surface density of ~300 molecules/μm^2. As shown in the line trace, single ICAM-1 molecules appear to have a height of 3.6 ± 0.7 nm and lateral dimension of 20 nm, due to tip broadening (Keller, 1991). To enhance the probability of detecting specific molecular interactions the ICAM-1 concentration in the adsorption process was increased, as is shown in Fig. 1 *b*. The tapping mode image clearly shows that the surface concentration was increased to such an extent (1000–1500 molecules/μm^2) that most of the single molecules could not be imaged separately, even when it is taken into account that this image has been taken with a normal Si_3N_4 tip, so the tip broadening is larger than with an EBD tip. The aggregates observed are interpreted as clusters of only a few molecules that have the same height as in Fig. 1 *a*. Also, stacks of molecules can be observed, as can be seen from the line trace. Similar images were obtained with high damping forces of typically 50% (data not shown), indicating that the molecules are strongly adsorbed to the mica. Apparently adsorption of ICAM-1 to mica provides us with a stable sample, suitable for molecular recognition.

Simultaneous imaging of height and adhesion

Fig. 2 shows the simultaneous imaging of both topography (*a, c, e, g, i*) and adhesion (*b, d, f, h, j*) of ICAM-1 molecules, recorded with functionalized tips.

Fig. 2, *a* and *b* were recorded with a tip that was functionalized with the specific antibody F10.2, which recognizes the most distal extracellular domain of ICAM-1. Although lateral and height resolution were not high enough to resolve individual molecules, the topographical image (Fig. 2 *a*) shows surface distribution similar to the tapping mode image at high concentration (Fig. 1 *b*). The clusters of molecules can be discriminated from the mica substrate and also the brighter spots are interpreted as stacks of two molecules, as in Fig. 1 *b*. Heavy low-pass filtering, necessary to improve the signal-to-noise ratio, causes the image to be differentiated and it can thus not be used for absolute height information. In the corresponding adhesion image (Fig. 2 *b*) bright pixels are observed, indicating very high adhesion between tip and sample. Many of the bright pixels correspond with the clusters of molecules in the topographical image, indicating spatially resolved molecular recognition of antibody-antigen interaction. Because correlation between height (Fig. 2 *a*) and adhesion (Fig. 2 *b*) image is

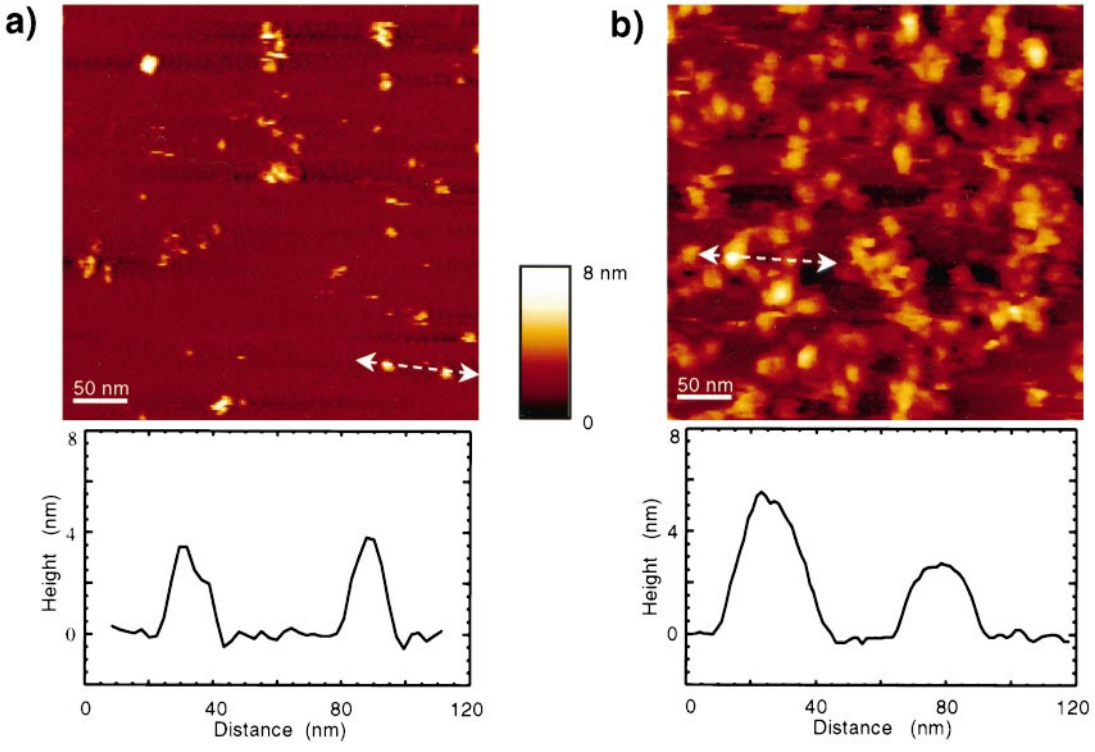

FIGURE 1 ICAM-1 adsorbed to mica, imaged in tapping mode in PBS at low (*a*) and high (*b*) concentration. Image size 400 × 400 nm, z-range 0–8 nm. Traces show the line-plots denoted by the arrows.

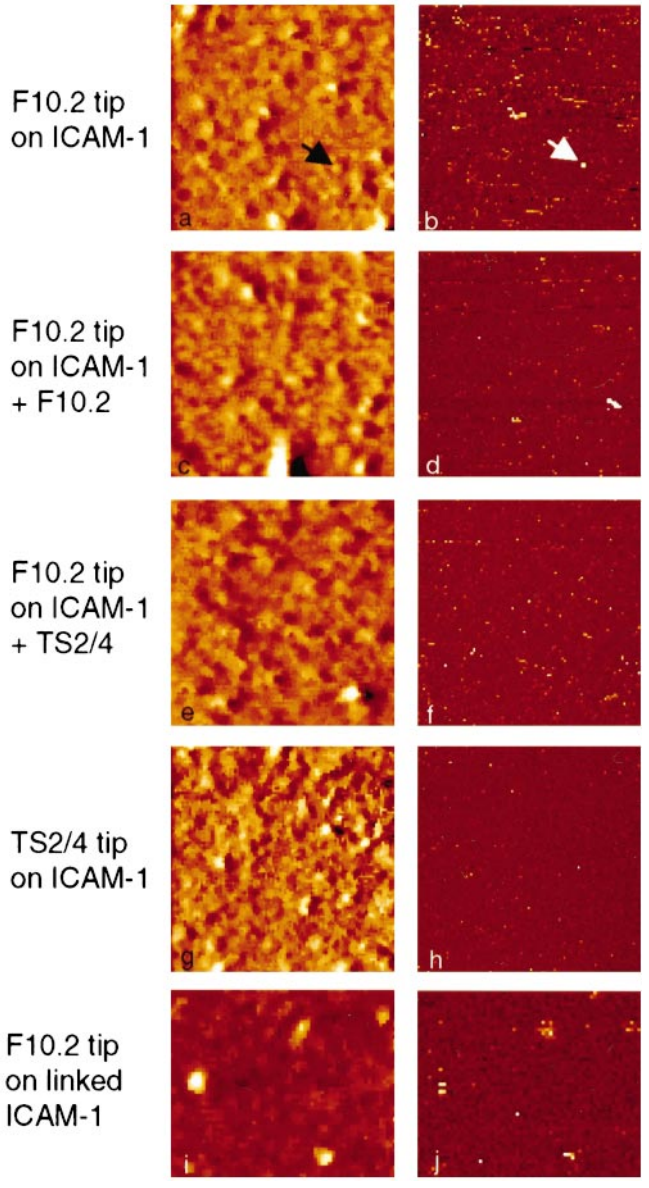

FIGURE 2 Simultaneously measured height (*a, c, e, g*) and adhesion (*b, d, f, g*) images of ICAM-1, adsorbed to mica, recorded in PBS with a functionalized tip. (*a* and *b*) F10.2 tip (anti-ICAM-1 tip). (*c* and *d*) F10.2 tip + F10.2 added (specific blocking step). (*e* and *f*) F10.2 tip + TS2/4 added ("nonspecific" blocking step). (*g* and *h*) TS2/4 tip (irrelevant antibody tip). Image size 400 × 400 nm, z-range 0–5 nm. Images (*i*) and (*j*) are simultaneously recorded height and adhesion image with an F10.2 tip on a modified mica substrate with low surface concentration ICAM-1. Image size is 250 × 200 nm, z-range 0–5 nm.

not clear, a high-resolution adhesion mode scan was taken on a sample of ICAM-1, bound to modified mica (see Materials and Methods). Fig. 2, *i* and *j* show the height and adhesion image of single ICAM-1 molecules with a scan size of 250 × 200 nm. The height image shows four individual ICAM-1 molecules of 20 nm on a flat substrate. The molecules have a height of 3–4 nm, which is the same as measured in Fig. 1, *a* and *b*, indicating that the newly developed force-distance mode is equally gentle to the molecules as the tapping mode. The adhesion image shows several bright pixels that match perfectly with the topographical image, gaining proof for the spatially resolved recognition process. In order to demonstrate that the bright spots were indeed mainly caused by specific interactions, we performed a number of control experiments.

In Fig. 2, *c–h* the control experiments to demonstrate the specificity of the antibody (F10.2)-antigen (ICAM-1) recognition are shown.

Fig. 2, *c* and *d* were recorded on the same position on the sample and with the same tip as Fig. 2, *a* and *b*, after addition of free F10.2 antibody to the solution. This should block the available binding sites on the adsorbed ICAM-1 molecules. The adhesion image (*d*) clearly shows that the number of adhesion peaks has decreased, indicating that the specific recognition is blocked by the antibodies in solution, while the topographical image (*c*) remains unchanged. Remaining bright pixels are attributed to nonspecific adhesion between tip and sample. The loss of specific adhesion events was not due to tip damage, as was checked by repeating the specific experiment on a fresh ICAM-1 sample, using the same tip. This was reproduced for several tips (data not shown).

Fig. 2, *e* and *f* are recorded with a tip, functionalized with the specific antibody F10.2, and the irrelevant antibody TS2/4 in solution during the measurement. This was done to show that the addition of an antibody in solution does not prevent the detection of recognition events. The topographical image shows surface distribution similar to the other experiments. The corresponding adhesion image shows that the number of adhesion peaks is lower than Fig. 2 *b*, which is attributed to the fact that this measurement is done with a new tip (b) that showed different nonspecific and specific adhesion from tip a. Table 1, however, indicates that the addition of TS2/4 to solution does not affect the molecular recognition process and that most of the bright pixels of Fig. 2 *f* indicate specific interactions.

Fig. 2, *g* and *h* are recorded with a tip, functionalized with the irrelevant antibody TS2/4 and an ICAM-1 sample. The topographical image shows a similar surface distribution as in the previous adhesion experiments. The adhesion image shows that almost no adhesion peaks appear, which agrees very well with the fact that the TS2/4 antibody cannot recognize ICAM-1. Because in addition to the height and adhesion image the total force-distance curve was recorded for every pixel, we can now analyze the force curves in detail.

Analysis of adhesion images

Fig. 3 shows typical force curves recorded with a functionalized tip at the ICAM-1 molecules under the various conditions described above.

Fig. 3, *a* and *b* show retraction curves from the force volume data, recorded simultaneously with Fig. 2, *a* and *b*. As expected, most of the curves did not show a detectable

TABLE 1 Interaction probabilities for all experiments

Tip/Substrate	Specific (%)	Nonspecific (%)	None (%)	Number of Curves
F10.2(a)/ICAM-1	10	10	80	2495
F10.2(a)/ICAM-1 + F10.2	3	5	92	2511
F10.2(b)/ICAM-1	6	12	82	2499
F10.2(b)/ICAM-1 + TS2/4	5	4	91	2501
F10.2(b)/ICAM-1 + TS2/4 + F10.2	1	24	75	2503
TS2/ 4 /ICAM-1	1	2	97	2501

unbinding force (see Fig. 3 *a*), due to the submonolayer surface coverage of ICAM-1. However, under conditions that specific interactions would be expected, 40% of the curves that were taken on top of the molecules (topographical images), look like Fig. 3 *b*. Finally, under all conditions curves that looked like Fig. 3 *c* are observed. The high-resolution adhesion image (Fig. 2 *j*) showed the same typical curves as shown in Fig. 3 *b*. It should be noted that no multiple unbinding events were observed during the curve analysis of this image, as can be expected from the interaction from a single antibody-antigen pair.

The difference between the curves of Fig. 3, *b* and *c* is that Fig. 3 *b* shows a change in slope during the retraction process, which is due to a decrease in effective spring constant. This change indicates that in the beginning of the retraction process, the cantilever is relaxed, while during further retraction, the complex of cantilever, spacer, F10.2, and ICAM-1 becomes stretched. In contrast to this, the curve of Fig. 3 *c* retains the same slope during the process of retraction. We attribute this to a nonspecific interaction between tip and substrate without the involvement of spacers, so only the cantilever is bent. In agreement with this explanation, these nonspecific interaction peaks account for the bright pixels in the adhesion images of the blocking experiments (Fig. 2, *d* and *h*), while they also account for a part of the bright pixels in Fig. 2, *b* and *f*.

The average value of the unbinding force of the specific interactions was 100 ± 50 pN. This value lies well within the range of binding strengths of other antibody-antigen interactions measured previously (Dammer et al., 1996; Hinterdorfer et al., 1996; Allen et al., 1997). From the unbinding curves a distribution of rupture lengths, as de-

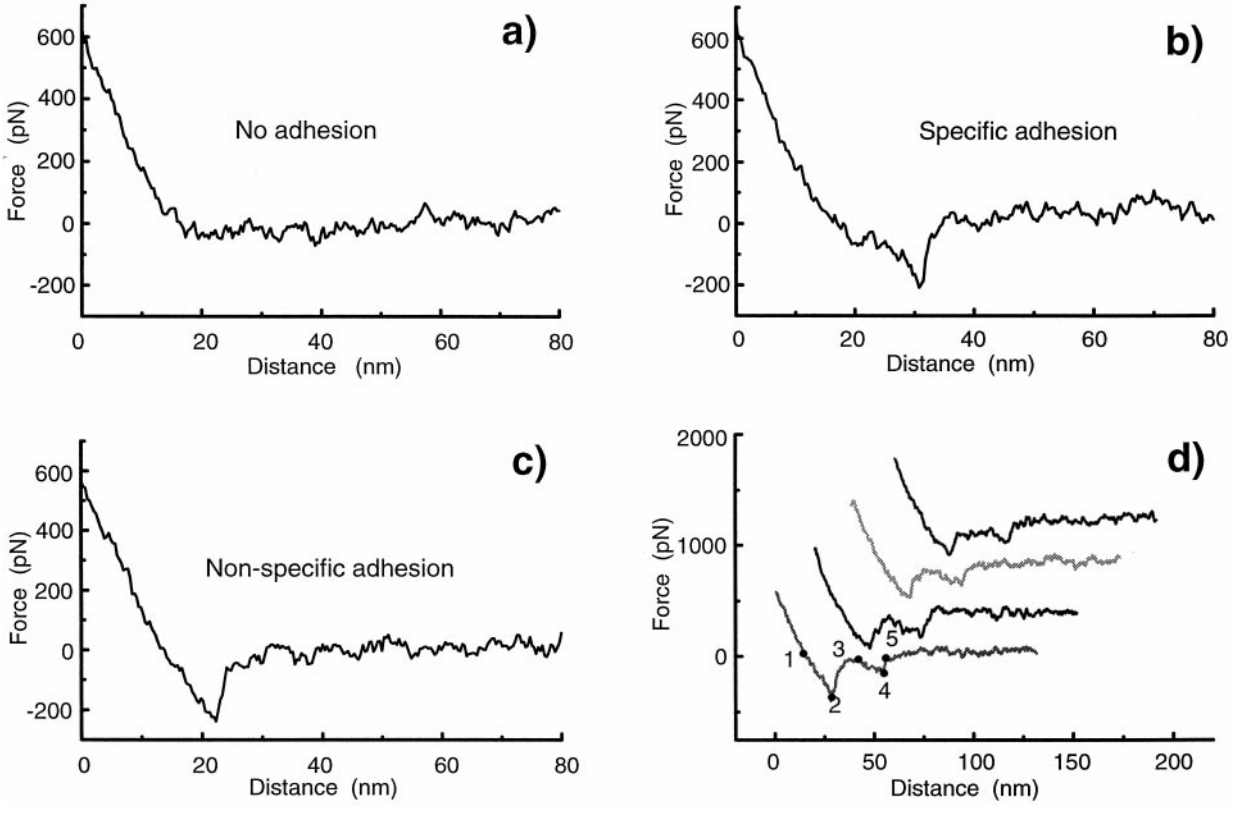

FIGURE 3 Typical retraction curves recorded simultaneously with Fig. 2, *a* and *b*. Trace (*a*) shows a curve without any detectable adhesion force, trace (*b*) shows a typical specific interaction, and trace (*c*) shows a typical nonspecific interaction. (*b*) shows a characteristic change in slope, due to stretching of the spacer-antibody-antigen complex; (*d*) shows four retraction curves, recorded at the position, indicated by the arrow in Fig. 2, *a* and *b*.

scribed earlier (Hinterdorfer et al., 1996), was calculated. The rupture length is defined as the distance between the end of the tip and the surface at disruption, and the distribution of these rupture lengths can be expected to have two maximums when the antibody is bound asymmetrically to the tip. The maximums represent the two Fab fragments of the F10.2 antibody that bind separately to ICAM-1. The distribution for the measurements of Fig. 2, *a* and *b* showed maximums at 11 and 16 nm, while other tips showed different rupture lengths (data not shown). This observation implies that in most of the specific curves only one Fab fragment of the complete antibody has recognized a single ICAM-1 molecule and that the rupture force measured, represents indeed the single molecular binding strength.

The arrow in Fig. 2, *a* and *b* points to a region of the sample where the four curves, depicted in Fig. 3 *d*, were taken. The four curves correspond to a square of four pixels in the adhesion image. These curves were taken on two subsequent scan lines and the time lapse between the first and fourth force curve is 8.5 s. It shows that our stand-alone head is stable enough to return to the same area of 64 nm^2 to measure a very similar unbinding process. Note that the area indicated in the adhesion image (Fig. 2 *b*) correlates with a cluster of ICAM-1 molecules in the topographical image (Fig. 2 *a*). The unbinding curves show that quantitative analysis is only possible with recording of the whole force-distance curve. All four curves show two unbinding processes. The first unbinding process (point 1 to 2) is caused by the same nonspecific interaction, as described above, while the second unbinding process (point 3 to 4) is caused by the stretching of the spacer-Ab-ICAM-1 complex, followed by the unbinding of F10.2 and ICAM-1 (point 4 to 5).

In Table 1 the unbinding process is quantified using the criteria mentioned above for selecting curves as specific, nonspecific, and no unbinding process. The binding probability is 10% (6% with tip b) for the specific interaction and goes down to 3% when F10.2 is added as a blocking agent. These two experiments were done with F10.2 tip a, while the nonspecific blocking by TS2/4 was carried out with F10.2 tip b. As can be seen from Table 1 this tip was also used for the original experiment to confirm specificity, after which TS2/4 was added for nonspecific blocking. From the table it can be seen that the interaction probability is not significantly affected by the presence of TS2/4.

DISCUSSION AND CONCLUSIONS

For the first time topography and adhesion are measured simultaneously with a resolution of 20 and 5 nm, respectively. Taking into account that the ICAM-1 molecules are only 18.7 nm long (Staunton et al., 1990), the resolution obtained in the height image is only limited by the convolution between the tip and molecule and thus allows single molecular height resolution. All experiments provide evidence that the force peaks in the adhesion image are mainly caused by single molecular interactions. This was enabled by combining the usage of a highly stable home-built AFM in adhesion mode (Van der Werf et al., 1994), together with a recently developed spacer technology, suitable for detecting single antibody-antigen recognition events (Hinterdorfer et al., 1996). The high-resolution height image showed individual ICAM-1 molecules that corresponded very well to bright adhesion pixels, thus indicating spatially resolved specific molecular recognition. The topographical image taken at a high surface concentration showed the contrast between clusters of ICAM-1 and the mica substrate, while the adhesion image shows many bright pixels on top of clusters of molecules, giving evidence to the molecular recognition process between individual ICAM-1 molecules and the antibody F10.2. Addition of blocking antibodies immediately causes a reduction of the number of specific interactions by 70%, while the surface distribution remains similar. All control experiments support the idea that single molecular interactions between ICAM-1 and F10.2 are measured.

It is still conceivable that the adhesion of Fig. 2 *j* is due to nonspecific interaction between the tip and the substrate. Analysis of the force curves of Fig. 2, *i* and *j* show that the spacer-antibody complex is clearly involved in the adhesion on the molecules. In principle it could still be a nonspecific interaction between the F10.2 antibody and the ICAM-1 antigen. However, the blocking experiment of Fig. 2 *d* makes this highly unlikely. Since the orientation of the ICAM-1 molecules is not altered by the photolinking step, which only fixes adsorbed molecules, we strongly believe that the control experiments shown in Fig. 2 also hold for the photolinked substrate.

EM images (Staunton et al., 1990) show sICAM-1 as a bent rod, 18.7 nm long, containing five immunoglobulin-like domains of $4 \times 2.5 \times 2.5$ nm. The tapping mode image with the low surface concentration (Fig. 1 *a*) and the adhesion mode topographical image (Fig. 2 *i*) show ICAM-1 as a round molecule of 3.5 nm height and a radius of 20 nm. Due to tip broadening, sample softness, and thermal movement of the ICAM-1 molecule it is impossible to resolve molecular substructure, as mentioned above, in physiological buffer (Hansma et al., 1995; Zhang et al., 1996).

When the topography images (Fig. 2, *a* and *i*) are compared to the adhesion images (Fig. 2, *b* and *j*), we note that the ICAM-1 molecules appear at least 400 nm^2 wide in topography, while they show an adhesion peak on typically three consecutive pixels, corresponding to 50 nm^2. Apparently successful binding does not occur every time the tip touches a molecule (40%). We attribute this to three effects. First of all, the F10.2 antibody has only a few milliseconds to find the ICAM-1 before it becomes retracted. During this period the antibody may not find the right orientation for the recognition process to occur, even when it is taken into account that the motility of the antibody is hardly restricted by the attachment to the spacer (Wong et al., 1997). Second, the adsorbed ICAM-1 can be oriented in such a way that the binding site is not accessible for the antibody. The third effect is illustrated by Fig. 4. When the tip, coated with

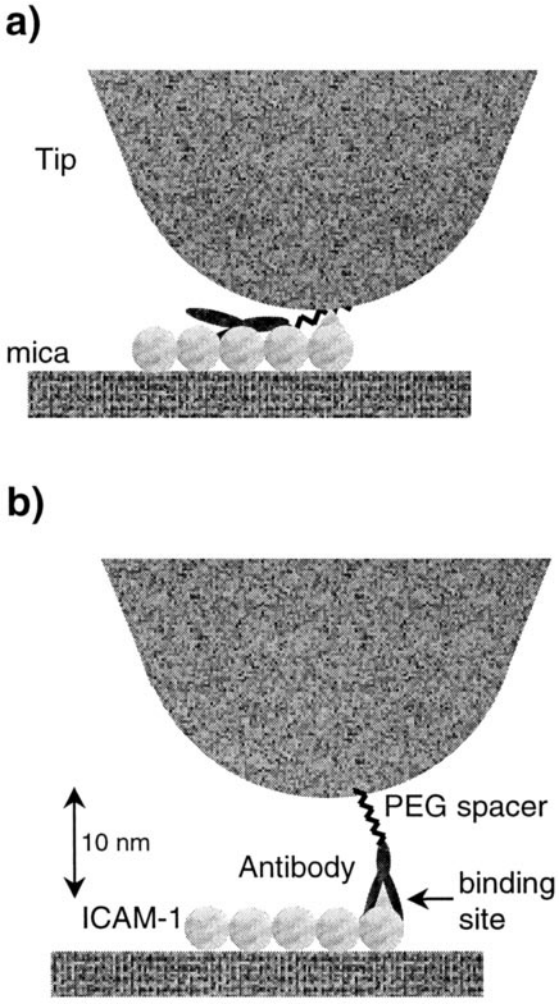

FIGURE 4 Schematic representation of the geometrical situation at height (*a*) and adhesion (*b*) measurement, which explains the tip and spacer convolution, respectively.

spacer and antibody, is pressed onto the surface, the tip surface touches the mica substrate or the ICAM-1. The topography (Fig. 4 *a*) is measured at maximal applied load, so the profile measured is a convolution between tip and ICAM-1, just as measured with a noncoated tip. Adhesion is measured (Fig. 4 *b*) by the interaction of the antigen of the surface with the antibody bound to the tip via a flexible cross-linker, so it does not involve the bare tip surface. The complex on the tip has the flexibility to reach the binding site on the surface within a lateral distance, equal to the dynamical reach of the spacer (Hinterdorfer et al., 1996; Hinterdorfer et al., 1998), which is in our case smaller (~6 nm) than the tip radius (~20 nm), so we might say that the adhesion image has a spacer convolution.

The force curves of specific interactions (Fig. 3, *b* and *d*) represent recognition events between individual antibody-antigen pairs. There are three reasons for this observation. First of all the mica substrate has been covered by a submonolayer of ICAM-1, as is shown in the tapping mode image (Fig. 1 *b*). This coverage minimizes the probability of antibodies on the tip to find several ICAM-1 molecules. Second, only 1% of the unbinding curves of Fig. 2 *b* shows two unbinding events, as might be expected from the fact that one particular antibody can bind to at most two molecules, while all other unbinding curves show single events. Moreover, all unbinding events taken on the low concentration sample exhibited only one unbinding event with the same rupture force, giving evidence that the measured force is indeed caused by a monovalent interaction. The double interactions can be separated from the monovalent interactions because both Fab fragments exhibit a different rupture length, being 5 nm apart for F10.2 tip (a). The double interactions might be caused by interaction of a single antibody with an ICAM-1 dimer. The sICAM-1, as used in this study, most likely is monomeric at the concentrations used for adsorption (Staunton et al., 1990; Miller et al., 1995). However, because of insufficient lateral resolution we cannot exclude the possibility that it forms dimers when adsorbing a high concentration to a surface. Finally, the surface coverage of F10.2 antibody on the tip is so low that the number of antibodies available for interactions with the ICAM-1 is 0.75 per tip. This estimated calculation agrees very well with the fact that not all modified tips showed the desired specificity. Moreover, the comparison between the two modified tips a and b in Table 1 shows that the interaction probability in the recognition experiment is not the same. If the number of available antibodies per tip is indeed lower than one on average, clearly not every spacer is attached to the tip at a geometrical equally favorable place, so not every antibody has the same chance to find its antigen. This low surface concentration makes it very unlikely to have more than one antibody on the tip, and is thus in agreement with the fact that single molecular interactions are observed.

In Fig. 3 *d* it is shown that it is possible to access the same molecule from four different positions, 6 nm apart. When the experiment is repeated for a number of times on the same position, one could calculate the spatial binding probability. In this way it is possible to determine the most probable location of the binding site of a molecule, as already shown in linear scans (Hinterdorfer et al., 1996). This, in combination with topography imaging, is a powerful tool for cell biological research. At present much effort is spent to improve the stability of the set-up so that it allows imaging the same molecule for several consecutive images.

Analysis of the force curves (Fig. 3, Table 1) indicates that the adhesion images have a certain background level of nonspecific interaction between sample and tip. This can be detected by the simultaneous force curve recording, which enables us to spatially separate the specific and nonspecific interactions (see Fig. 3 *d*). Discrimination between specific and nonspecific interactions is possible due to the use of spacer technology. We observed that a freshly modified tip showed an increase in the number of nonspecific interactions after typically 20,000 force curves, making the tip useless as an imaging tool, although it was still biochemically intact. This observation is illustrated in Table 1, in

which the third experiment with tip b (F10.2(b)/ICAM-1 + TS2/4 + F10.2) exhibits an increase in the number of nonspecific interactions. Also, different batches of tips showed a different number of nonspecific interactions. We found that the number of nonspecific interactions could be modulated by the applied force. This can be explained by the Hertz model (Israelachvili, 1991), which states that the contact area between tip and sample depends on the force by a power of ⅔, so an increase in the force will increase the probability of nonspecific interactions. However, at forces below 100 pN the topographical image quality decreased dramatically. By working with sharp, chemically well-defined tips and ultralow forces, the background of nonspecific interactions could be reduced to such an extent that the on-line adhesion imaging would provide us with direct and fast information on the location of the specific adhesive sites on, for instance, a cell surface.

We thank Dr. A. C. Bloem for kindly providing antibodies, Minke Binnerts for the sICAM-1 construct, Karin Haarhuis for the purification of sICAM-1, and Bert Otter for providing e-beam deposited tips. We thank John van Noort and Niek van Hulst for helpful discussions.

This research was supported by the Dutch Technology Foundation (STW).

REFERENCES

Allen, S., X. Chen, J. Davies, M. C. Davies, A. C. Dawkes, J. C. Edwards, C. J. Roberts, J. Sefton, S. J. B. Tendler, and P. M. Williams. 1997. Detection of antigen-antibody binding events with the atomic force microscope. *Biochemistry.* 36:7457–7463.

Berger, C. E. H., K. O. van der Werf, R. P. H. Kooyman, B. G. de Grooth, and J. Greve. 1995. Functional group imaging by adhesion AFM applied to lipid monolayers. *Langmuir.* 11:4188–4192.

Binnig, G., C. F. Quate, and C. Gerber. 1986. Atomic force microscope. *Phys. Rev. Lett.* 56:930–933.

Binnig, G., H. Rohrer, C. Gerber, and E. Weibel. 1983. 7 × 7 Reconstruction on Si(111) resolved in real space. *Phys. Rev. Lett.* 50:120–123.

Bloemen, P., G. Moldenhauer, M. van Dijk, H. J. Schuurman, and A. C. Bloem. 1992. Multiple ICAM-1 (CD54) epitopes are involved in homotypic B-cell adhesion. *Scand. J. Immunol.* 35:517–523.

Butt, H.-J., and M. Jaschke. 1995. Calculation of thermal noise in atomic force microscopy. *Nanotechnology.* 6:1–7.

Dammer, U., M. Hegner, D. Anselmetti, P. Wagner, M. Dreier, W. Huber, and H.-J. Güntherodt. 1996. Specific antigen/antibody interactions measured by force microscopy. *Biophys. J.* 70:2437–2441.

Dammer, U., O. Popescu, P. Wagner, D. Anselmetti, H.-J. Güntherodt, and G. N. Misevic. 1995. Binding strength between cell adhesion proteoglycans measured by atomic force microscopy. *Science.* 267:1173–1175.

De Grooth, B. G., and C. A. J. Putman. 1992. High-resolution imaging of chromosome-related structures by atomic force microscopy. *J. Microsc.* 168:239–247.

Diamond, M. S., and T. A. Springer. 1994. The dynamic regulation of integrin adhesiveness. *Curr. Biol.* 4:506–517.

Figdor, C. G., Y. Van Kooyk, and G. D. Keizer. 1990. On the mode of action of LFA-1. *Immunol. Today.* 11:277–280.

Florin, E.-L., V. T. Moy, and H. E. Gaub. 1994. Adhesion forces between individual ligand-receptor pairs. *Science.* 264:415–417.

Florin, E.-L., M. Rief, H. Lehmann, M. Ludwig, C. Dornmair, V. T. Moy, and H. E. Gaub. 1995. Sensing specific molecular interactions with the atomic force microscope. *Biosens. Bioelectron.* 10:895–901.

Hansma, P. K., J. P. Cleveland, M. Radmacher, D. A. Walters, P. E. Hillner, M. Bezanilla, M. Fritz, D. Vie, H. G. Hansma, C. B. Prater, J. Massie, L. Fukunaga, J Gurley, and V. Elings. 1994. Tapping mode atomic force microscopy in liquids. *Appl. Phys. Lett.* 64:1738–3740.

Hansma, H. G., D. E. Laney, M. Bezanilla, R. L. Sinsheimer, and P. K. Hansma. 1995. Applications for atomic force microscopy of DNA. *Biophys. J.* 68:1672–1677.

Haselgrübler, Th., A. Amerstorfer, H. Schindler, and H. J. Gruber. 1995. Synthesis and applications of a new poly(ethylene glycol) derivative for the crosslinking of amines with thiols. *Bioconjugate Chem.* 6:242–248.

Henderson, E., P. G. Haydon, and D. S. Sakaguchi. 1992. Actin filament dynamics in living glial cells imaged by atomic force microscopy. *Science.* 257:1944–1946.

Hinterdorfer, P., W. Baumgartner, H. J. Gruber, K. Schilcher, and H. Schindler. 1996. Detection and localization of individual antibody-antigen recognition events by atomic force microscopy. *Proc. Natl. Acad. Sci. USA.* 93:3477–3481.

Hinterdorfer, P., K. Schilcher, W. Baumgartner, H. J. Gruber, and H. Schindler. 1998. A mechanistic study of the dissociation of individual antibody-antigen pairs by atomic force microscopy. *Nanobiology.* 4:39–50.

Hoh, J. H., J. P. Cleveland, C. B. Pratter, J.-P. Revel, and P. K. Hansma. 1992. Quantized adhesion detected with the atomic force microscope. *J. Am. Chem. Soc.* 114:4917–4918.

Hynes, R. O. 1992. Integrins: versatility, modulation, and signaling in cell adhesion. *Cell.* 69:11–25.

Israelachvili, J. N. 1991. Intermolecular and Surface Forces. 2nd ed. Academic Press, London.

Kasas, S., N. H. Thomson, B. L. Smith, H. G. Hansma, X. Zhu, M. Guthold, C. Bustamante, E. T. Kool, M. Kashlev, and P. K. Hansma. 1997. *Escherichia coli* RNA polymerase activity observed using Atomic Force Microscopy. *Biochemistry.* 36:461–468.

Keller, D. 1991. Reconstruction of STM and AFM images distorted by finite-size tips. *Surf. Sci.* 253:353–364.

Keller, D., and C. Chic-Chung. 1992. Imaging steep, high structures by scanning force microscopy with electron beam deposited tips. *Surf. Sci.* 268:333–339.

Lee, G. U., L. A. Chris, and R. J. Colton. 1994b. Direct measurement of the forces between complementary strands of DNA. *Science.* 266:771–773.

Lee, G. U., D. A. Kidwell, and R. J. Colton. 1994a. Sensing discrete streptavidin-biotin interactions with atomic force microscopy. *Langmuir.* 10:354–357.

Lub, M., Y. van Kooyk, and C. Figdor. 1995. Ins and outs of LFA-1. *Immunol. Today.* 16:479–483.

Ludwig, M., W. Dettmann, and H. E. Gaub. 1997. Atomic force microscope imaging contrast based on molecular recognition. *Biophys. J.* 72:445–448.

Marti, O., B. Drake, and P. K. Hansma. 1987. Atomic force microscopy of liquid-covered surfaces: atomic resolution images. *Appl. Phys. Lett.* 51:484–486.

Miller, J., R. Knorr, M. Ferrone, R. Houdei, C. P. Carron, and M. L. Dustin. 1995. Intercellular adhesion molecule-1 dimerization and its consequences for adhesion mediated by lymphocyte function associated-1. *J. Exp. Med.* 182:1231–1241.

Moy, V. T., E. L. Florin, and H. E. Gaub. 1994. Intermolecular forces and energies between ligands and receptors. *Science.* 266:257–259.

Putman, C. A. J., K. O. van der Werf, B. G. de Grooth, N. F. van Hulst, and J. Greve. 1994. Viscoelasticity of living cells allows high resolution imaging by tapping mode atomic force microscopy. *Biophys. J.* 67: 1749–1753.

Radmacher, M., J. P. Cleveland, M. Fritz, H. G. Hansma, and P. K. Hansma. 1994b. Mapping interaction forces with the atomic force microscope. *Biophys. J.* 66:2159–2165.

Radmacher, M., M. Fritz, H. G. Hansma, and P. K. Hansma. 1994a. Direct observation of enzyme activity with the atomic force microscope. *Science.* 265:1577–1579.

Rief, M., M. Gautel, F. Oesterhelt, J. M. Fernandez, and H. E. Gaub. 1997b. Reversible unfolding of individual titin immunoglobulin domains by AFM. *Science.* 276:1109–1112.

Rief, M., F. Oesterhelt, B. Heymann, and H. E. Gaub. 1997a. Single molecule force spectroscopy on polysaccharides by atomic force microscopy. *Science.* 275:1295–1297.

Sanchez-Madrid, F., A. M. Krensky, C. F. Ware, E. Robbins, J. L. Strominger, S. J. Burakoff, and T. A. Springer. 1982. Three distinct

antigens associated with human T-lymphocyte-mediated cytolysis: LFA-1, LFA-2, and LFA-3. *Proc. Natl. Acad. Sci. USA.* 79:7489–7493.

Schmidt, Th., G. J. Schütz, W. Baumgartner, H. J. Gruber, and H Schindler. 1996. Imaging of single molecule diffusion. *Proc. Natl Acad. Sci. USA.* 93:2926–2929.

Staunton, D. E., M. L. Dustin, H. P. Erickson, and T. A. Springer. 1990. The arrangement of the immunoglobulin-like domains of ICAM-1 and the binding sites for LFA-1 and rhinovirus. *Cell.* 61:243–254.

van der Werf, K. O., C. A. J. Putman, B. G. de Grooth, and J. Greve. 1994. Adhesion force imaging in air and liquid by adhesion mode atomic force microscopy. *Appl. Phys. Lett.* 65:1195–1197.

van der Werf, K. O., C. A. J. Putman, B. G. de Grooth, F. B. Segerink, E. H. Schipper, N. F. van Hulst, and J. Greve. 1993. Compact standalone atomic force microscope. *Rev. Sci. Instrum.* 64:2892–2897.

Wong, J. Y., T. L. Kuhl, J. N. Israelachvili, N. Mullah, and S. Zalipsky. 1997. Direct measurement of a tethered ligand-receptor interaction potential. *Science.* 275:820–822.

Zhang, Y., S. Sheng, and Z. Shao. 1996. Imaging biological structures with the cryo atomic force microscope. *Biophys. J.* 71:2168–2176.

Zhong, Q., D. Inniss, K. Kjoller, and V. B. Elings. 1993. Fractured polymer/silica fiber surface studied by tapping mode atomic force microscopy. *Surf. Sci. Lett.* 290:688.